Spin- and pseudospin-polarized quantum Hall liquids in HgTe quantum wells

Kh. Shakouri and F. M. Peeters
Departement Fysica, Universiteit Antwerpen, Groenenborgerlaan 171, B-2020 Antwerpen, Belgium
(Received 4 February 2015; published 17 July 2015)

A Hg(Cd)Te insulator heterostructure hosts a two-dimensional electron system that can simulate the physics of Dirac fermions with only a single valley. We investigate the magnetotransport properties of this structure and show that, unlike most two-dimensional crystals with spin and valley coupled levels, the Shubnikov–de Haas oscillations exhibit a high spin polarization in the absence of any valley degree of freedom. This effect can be observed using magnetospectroscopy measurements for quantum well thicknesses corresponding to either the topologically trivial or quantum spin Hall phases. The pseudospin texture of the electrons near the Fermi level is also studied and we show that a tunable pseudospin-polarized quantum Hall liquid can only be observed for thicknesses corresponding to the inverted regime.

DOI: 10.1103/PhysRevB.92.045416 PACS number(s): 72.25.−b, 71.70.Di, 73.43.−f, 75.47.−m

I. INTRODUCTION

The recently discovered conductive boundary states in topological insulators (TIs) have opened up new prospects for the investigation of novel electronic states [1–9]. A key characteristic of these Dirac-like nontrivial states stems from their insensitivity to spin-independent scattering. Physically, such a state is robust against localization or backscattering by nonmagnetic impurities because of time-reversal invariance [4,6]. As a consequence, TIs host dissipationless transport channels with potentially novel properties that can be engineered for low-power electronics and spintronics.

Soon after the anticipation of topological states in HgTe quantum wells (QWs) [1]—a superimposed HgTe/(Hg,Cd)Te heterostructure—the predicted gapless edge modes were experimentally observed [2]. The existence of these nontrivial modes is highly sensitive to the QW thickness d [1]. When d exceeds a critical value d_c, the band ordering of the Γ_6 electron and Γ_8 hole bands of the HgTe QW is energetically inverted, leading to a phase transition between the topologically trivial and quantum spin Hall (QSH) regimes. In the QSH regime, the edge states exhibit quantized conductance plateaus, in the absence of any external magnetic field, which have a distinct helical property: the Kramers' doublets with opposite spins propagate in opposite directions. Nevertheless, the survival of the helical states is locked to the spin dephasing length [10] and they have been predicted to be localized or affected by a randomly spatially fluctuating Rashba spin-orbit interaction [11] or impurities [12].

At the critical thickness d_c, the physics of massless Dirac fermions with linear dispersion emerges which recently has been confirmed experimentally [13]. In this case, unlike topological crystalline insulators [14] and most two-dimensional (2D) materials in which all Dirac fermions are labeled by their valley index, a HgTe QW behaves like a half graphene with only a single valley [13]. This property can be considered as an advantage because the interplay of valley and spin degrees of freedom usually imposes rigorous constraints against spin- or valley-polarized excitations, especially in magneto-optical transport. In Ref. [13], the transport properties of HgTe QWs have been investigated both theoretically and experimentally for $d = d_c$, but the presented theory only focuses on the conductivity coefficients in the absence of a magnetic field. In the present work, we study theoretically the magnetotransport properties of HgTe QWs and show that a fully spin-polarized quantum Hall liquid is predicted to be observable in both the topologically trivial and inverted regimes. Such a high-efficiency spin polarization can be detected experimentally in Shubnikov–de Haas oscillations and leads to a splitting of several meV which lies in the detectable range of magnetospectroscopy measurements that have previously been performed on graphene [15,16]. Moreover, it is shown that although the magnetic field forces both the ordinary and inverted phases into a spin-polarized quantum Hall regime, the pseudospin degree of freedom can still be viewed as a characteristic separating between these topologically distinct phases.

II. MODEL AND SPECTRUM

The electronic states of HgTe QWs—near the Γ point in the Brillouin zone—are described by the B-H-Z model Hamiltonian [1] derived from 8-band $k\cdot p$ theory [17]. In the basis of $|E_1,1/2\rangle$, $|H_1,3/2\rangle$, $|E_1,-1/2\rangle$, and $|H_1,-3/2\rangle$ subbands, the Hamiltonian is block diagonal with respect to the spin degree of freedom:

$$H=\begin{bmatrix} h(k) & 0 \\ 0 & h^*(-k)\end{bmatrix}, \tag{1}$$

where $h(k)=\mathcal{C}-\mathcal{D}k^2+\mathbf{d}_k\cdot\vec{\tau}$ and $h^*(-k)$ are for spin-up and spin-down, respectively, $\vec{\tau}$ is the vector of Pauli matrices associated with the pseudospin degree of freedom for E_1 and H_1 subbands, $\mathbf{d}_k=[\mathcal{A}k_x,-\mathcal{A}k_y,\mathcal{M}-\mathcal{B}k^2]$, $\mathcal{M}$ is the Dirac mass (or gap) parameter, and $\mathcal{C}$, $\mathcal{D}$, $\mathcal{B}$, and $\mathcal{A}$ are system parameters given in Table I. The mass parameter $\mathcal{M}$ changes its sign at $d=d_c$, leading to a closure of the bulk insulating gap. With the presence of an external magnetic field $\mathbf{B}=B\hat{e}_z$ the exact solution to model (1) gives the following Landau level (LL) dispersion:

$$E^s_{n\alpha}=-\frac{2}{\ell_B^2}n\mathcal{D}+\frac{s}{\ell_B^2}\mathcal{B}+\alpha\sqrt{\left(\mathcal{M}-\frac{2}{\ell_B}n\mathcal{B}+\frac{s}{\ell_B}\mathcal{D}\right)^2+\frac{2}{\ell_B^2}n\mathcal{A}^2}, \tag{2}$$

TABLE I. Material parameters for Hg(Cd)Te QWs [18].

d (Å)	$\mathcal{A}$ (eV Å)	$\mathcal{B}$ (eV Å^2)	$\mathcal{D}$ (eV Å^2)	$\mathcal{M}$ (meV)
55	3.87	−48.0	−30.6	9
70	3.65	−68.6	−51.2	−10

where $\ell_B = (eB/\hbar)^{-1/2}$ is the magnetic length, $n \geqslant 1$ the LL index, $s = \pm 1$ the spin quantum number, and $\alpha = +/-$ specifies the electron/hole states. Here, we omitted the contribution due to the Zeeman-type term because the main g factor comes from the orbital effects that are incorporated in Eq. (1) [13]. For the zeroth LL, the energy is given by $E^s_{n=0} = -s\mathcal{M} + \frac{1}{\ell_B^2}(s\mathcal{B} - \mathcal{D})$; thus the crossing of the zero-mode spins occurs at $B = \hbar\mathcal{M}/e\mathcal{B}$. Using the Landau gauge $\vec{A} = Bx\,\hat{j}$, the associated eigenstates can formally be written in the basis of the quantum oscillator, ϕ_n, as $\Psi(x,y) = L_y^{-\frac{1}{2}} e^{ik_y y}[a^s_{n\alpha}\phi_{n-1}(u), b^s_{n\alpha}\phi_n(u)]^T$ for $s = 1$ and $u = x/\ell_B + \ell_B k_y$. For $s = -1$, the components are interchanged. Also, the coefficients of the spinors are defined as $(a^s_{n\alpha}, b^s_{n\alpha}) = (c^2 + 2n\mathcal{A}^2/\ell_B^2)^{-\frac{1}{2}}(c, i\sqrt{2n}\mathcal{A}/\ell_B)$ with $c = sE^s_{n\alpha} + \mathcal{M} - \frac{2}{\ell_B^2}(\mathcal{B} - s\mathcal{D})(n + 1/2)$.

The ability to control the pseudospin direction by means of a magnetic field is only feasible for the inverted regime. The expectation value of subband pseudospin, evaluated for a few low-lying LLs with $\alpha > 0$, is illustrated in Figs. 1(a) and 1(b) for $d = 55$ Å and $d = 70$ Å. Owing to the coupling between pseudospin and orbital degrees of freedom, the index τ is not a good quantum number. For sufficiently weak magnetic fields, the direction of $\langle\tau_z\rangle$ ($\langle\tau_x\rangle = \langle\tau_y\rangle = 0$) is opposite for the ordinary ($d = 55$ Å) and inverted ($d = 70$ Å) regimes. By contrast, for strong magnetic fields, the pseudospin direction can be reversed for $d = 70$ Å—the inversion occurs at $B = \hbar\mathcal{M}/[e(2n\mathcal{B} - s\mathcal{D})]$ except for the zero-mode LL which is fully pseudospin-polarized—while this effect never occurs

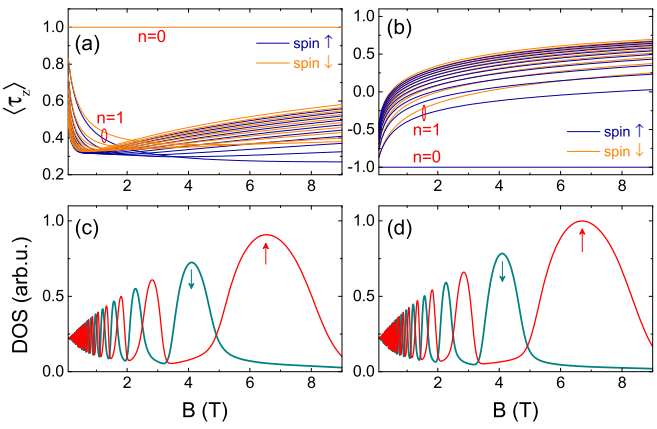

FIG. 1. (Color online) (a), (b) The expectation value of pseudospin for the few lowest LLs for $d = 55$ Å ($d < d_c$) and $d = 70$ Å ($d > d_c$), respectively. In the inverted regime with $d_c < d$, the pseudospin direction is opposite and changes its sign with increasing magnetic field except for the zeroth level $n = 0$. (c), (d) The density of opposite spin states near the Fermi level as a function of the magnetic field for $d = 55$ Å and $d = 70$ Å, respectively.

for the case of ordinary insulator even by reversing the field B. As will be shown next, this allows one to tune the pseudospin transport via the density of charge carriers, for only $d = 70$ Å. However, there is still a shared feature and that is the similarity in the spin behavior; see, e.g., Figs. 1(c) and 1(d) for the Fermi level density of states (DOS) where the details of the calculations are given in the following.

III. MAGNETOTRANSPORT

In the absence of any edges, which give rise to transport channels, an external magnetic field can confine the electrons in cyclotron orbits which demands an absolutely perfect system. In contrast, the scattering processes such as nonlocal random impurities or disorder provide the electrons the opportunity to change their initial orbit, resulting in the conduction of carriers at low temperatures. We calculate this contribution within linear response theory by using the Kubo formula [19,20]. The longitudinal dc conductivity of an isotropic system is given by [21]

$$\sigma_{xx} = \pi e^2\hbar \int d\varepsilon \left(-\frac{\partial f}{\partial \varepsilon}\right) \int \frac{d^2\mathbf{q}}{(2\pi)^2} \times \sum_{\zeta\zeta'} \langle\zeta|\hat{v}_x A(\mathbf{q},E)|\zeta'\rangle\langle\zeta'|\hat{v}_x A(\mathbf{q},E)|\zeta\rangle. \quad (3)$$

Here, ζ runs over all quantum numbers n, α, s, and k_y, and $\hat{v}_x$ is the x projection of the velocity operator $\hat{\mathbf{v}} = \nabla_{\mathbf{p}} H$ with $\mathbf{p}$ being the kinetic momentum. The evaluation of the spectral function $A(\mathbf{q}, E)$ is straightforward in view of the treatment detailed in Ref. [22]. We begin with the case of an unperturbed system and represent the retarded propagator $G^{0r}(\mathbf{r}_1, \mathbf{r}_2, E)$ in the center of mass and relative coordinates [23], $\mathbf{R} = \frac{1}{2}(\mathbf{r}_1 + \mathbf{r}_2)$ and $\mathbf{r} = \mathbf{r}_1 - \mathbf{r}_2$, which is called the Wigner transformation. This gives

$$G^{0r}(\mathbf{q},\mathbf{R},E) = \sum_\zeta \int_{-\infty}^{\infty} e^{-i\mathbf{q}.\mathbf{r}} \frac{\langle \mathbf{R} + \frac{1}{2}\mathbf{r}|\zeta\rangle\langle\zeta|\mathbf{R} - \frac{1}{2}\mathbf{r}\rangle}{E - E_\zeta + i\eta} d\mathbf{r}, \quad (4)$$

where η is an infinitesimal real constant and $\langle \mathbf{R} + \frac{1}{2}\mathbf{r}|\zeta\rangle = \Psi_\zeta(\mathbf{R} + \frac{1}{2}\mathbf{r})$, etc. Substituting the eigenstates for $\zeta = |n,\alpha,s,k_y\rangle$, Eq. (4) can be cast into the following form [24]:

$$G^{0r}_s(q,E) = \sum_{n,\alpha} \frac{2(-1)^n e^{-\ell_B^2 q^2}}{E - E^s_{n\alpha} + i\eta} \left[|b^s_{n\alpha}|^2 L_n(2\ell_B^2 q^2) - |a^s_{n\alpha}|^2 L_{n-1}(2\ell_B^2 q^2)\right], \quad (5)$$

where L_n is the Laguerre polynomial. Notice that the transport Green's function $G^{0r}_s(q,E)$ accounts for only the pure states without disorder. The disorder in the system is considered as being spatial fluctuations in the QW thickness, around the average thickness d, which are distributed randomly (see the supplementary online information in Ref. [13]). This type of disorder perturbs mainly the effective mass term $\mathcal{M}$, resulting in slight deviations $\sum_{i=1}^{N_d} \delta\mathcal{M}(\mathbf{r} - \mathbf{r}_i)$ at random positions $\mathbf{r}_i$. In accordance with common models, we assume $\delta\mathcal{M}(r) = \mathcal{M}_0 e^{-r^2/2r_0^2}$ where $\mathcal{M}_0$ denotes the maximum deviation of $\mathcal{M}$, for each fluctuation, and r_0 specifies the Gaussian width. We switch to dimensionless Fourier space $\ell_B q \to q$, for

simplicity, and adopt the self-consistent Born approximation by which the self-energy is expressed as

$$\Sigma_s^r(\mathbf{q},E)=\int\frac{d\mathbf{q}'}{(2\pi)^2}v(\mathbf{q}-\mathbf{q}')G_s^r(\mathbf{q}',E)v(\mathbf{q}'-\mathbf{q}). \quad (6)$$

Here, $v(\mathbf{q})=\mathcal{F}_{\mathbf{r}}[\sum_{i=1}^{N_d}\delta\mathcal{M}(\mathbf{r}-\mathbf{r}_i)]$ is the Fourier transform of the disorder potential. It can be proven that $|v(q)|^2\approx N_d|\delta\mathcal{M}(q)|^2$, with $\delta\mathcal{M}(q)=2\pi\ell_B^2\gamma\mathcal{M}_0e^{-\gamma q^2/2}$ and $\gamma=r_0^2/\ell_B^2$, provided that N_d is very large. Therefore, the self-energy (6) becomes

$$\Sigma_s^r(\mathbf{q},E)=N_d\int\frac{d\mathbf{q}'}{(2\pi)^2}[\delta\mathcal{M}(|\mathbf{q}-\mathbf{q}'|)]^2G_s^r(\mathbf{q}',E). \quad (7)$$

Starting with the unperturbed Green's function (5), in the first iteration we obtain (cf. Ref. [25])

$$\int e^{-\gamma(\mathbf{q}-\mathbf{q}')^2}e^{-q'^2}L_n(2q'^2)d\mathbf{q}'$$
$$=\pi\frac{(-1)^n}{1+\gamma}\left(\frac{1-\gamma}{1+\gamma}\right)^n e^{-\frac{\gamma}{1+\gamma}q^2}L_n\left(-\frac{2\gamma^2q^2}{1-\gamma^2}\right). \quad (8)$$

For long-range disorder with $\gamma\gg1$ and finite n, the above equation readily renders $\pi\gamma^{-1}e^{-q^2}L_n(2q^2)$ which has a similar form to the initial (starting) function. Since the Gaussian broadening $e^{-\gamma(\mathbf{q}-\mathbf{q}')^2}$ peaks around $\mathbf{q}=\mathbf{q}'$, this allows us to write the disorder-averaged self-energy as $\Sigma_s^r(q,E)\approx\Gamma(\hbar\omega_c)^2G_s^r(q,E)$ with $\Gamma=\pi N_d\gamma\mathcal{M}_0^2/\hbar^2\omega_c^2$ the field-independent dimensionless parameter determining the disorder strength. The spectral function then becomes

$$A_s(q,E)=-\frac{2e^{-q^2}}{\pi}\sum_{n,\alpha}(-1)^n\mathcal{L}_{n\alpha}^s(E)\left[\left|b_{n\alpha}^s\right|^2L_n(2q^2)\right.$$
$$\left.-\left|a_{n\alpha}^s\right|^2L_{n-1}(2q^2)\right], \quad (9)$$

where $\mathcal{L}_{n\alpha}^s(E)=\mathrm{Im}\,\Sigma_s^r/[(E-E_{n,\alpha}^s-\mathrm{Re}\,\Sigma_s^r)^2+(\mathrm{Im}\,\Sigma_s^r)^2]$ is a Lorentzian-type broadening. Notice that the DOS per unit area is proportional to this function, $D(E)=\frac{1}{2\pi\ell_B^2}\times-\frac{1}{\pi}\sum_{n,\alpha,s}\mathcal{L}_{n\alpha}^s(E)$, which can be proven by integrating over q in Eq. (9). Finally, using Eq. (9) together with the orthogonality property of Laguerre polynomials, the Kubo formula (3) takes the form

$$\sigma_{xx}^s=\frac{e^2\hbar}{\pi^2}\int\frac{d\varepsilon}{4K_BT\cosh^2\left(\frac{\varepsilon-E_F}{2K_BT}\right)}$$
$$\times\frac{-1}{\pi\ell_B^2}\sum_{n,\alpha}\left[\left(S_{n\alpha}^{n-1\alpha}\right)^2\left|a_{n\alpha}^s\right|^2\left|b_{n-1\alpha}^s\right|^2\mathcal{L}_{n\alpha}^s\mathcal{L}_{n-1\alpha}^s\right.$$
$$\left.+\left(S_{n+1\alpha}^{n\alpha}\right)^2\left|b_{n\alpha}^s\right|^2\left|a_{n+1\alpha}^s\right|^2\mathcal{L}_{n\alpha}^s\mathcal{L}_{n+1\alpha}^s\right], \quad (10)$$

where

$$S_{n\alpha}^{n'\alpha'}=\frac{1}{\hbar\ell_B}\left[\ell_B\mathcal{A}a_{n\alpha}^sb_{n'\alpha'}^s-ib_{n\alpha}^sb_{n'\alpha'}^s\sqrt{2n}(\mathcal{B}-\mathcal{D})\right.$$
$$\left.-ia_{n\alpha}^sa_{n'\alpha'}^s\sqrt{2n'}(\mathcal{B}+\mathcal{D})\right]. \quad (11)$$

A straight and general approach to calculate the contribution of the Hall component σ_{xy} is to use the Kubo-Greenwood formalism [19,20,26]. The resistivity components are then given by the inverse of the conductivity tensor as $\rho=\sigma^{-1}$.

Mapping the longitudinal resistivity in scales of the magnetic field and electron density results in the famous fan chart [27,28] with blades that spread with increasing magnetic field; see Figs. 2(a) and 2(b). The deep minima in strong magnetic fields, depicted by dark colors, occur indeed accompanied by vanishingly small DOS, e.g., near the crossings in Figs. 1(c) and 1(d) for $B>2$ T, which is a consequence of the large spacing between the LLs. For these regions, the resistivity oscillations appear as pronounced peaks indicating the advent of the Shubnikov–de Haas effect. The notable feature in this case is that the resonant peaks have a high spin resolution without any side effects due to the valley degrees of freedom as prevalent in most 2D crystals. This effect holds for both the normal (nontopological)

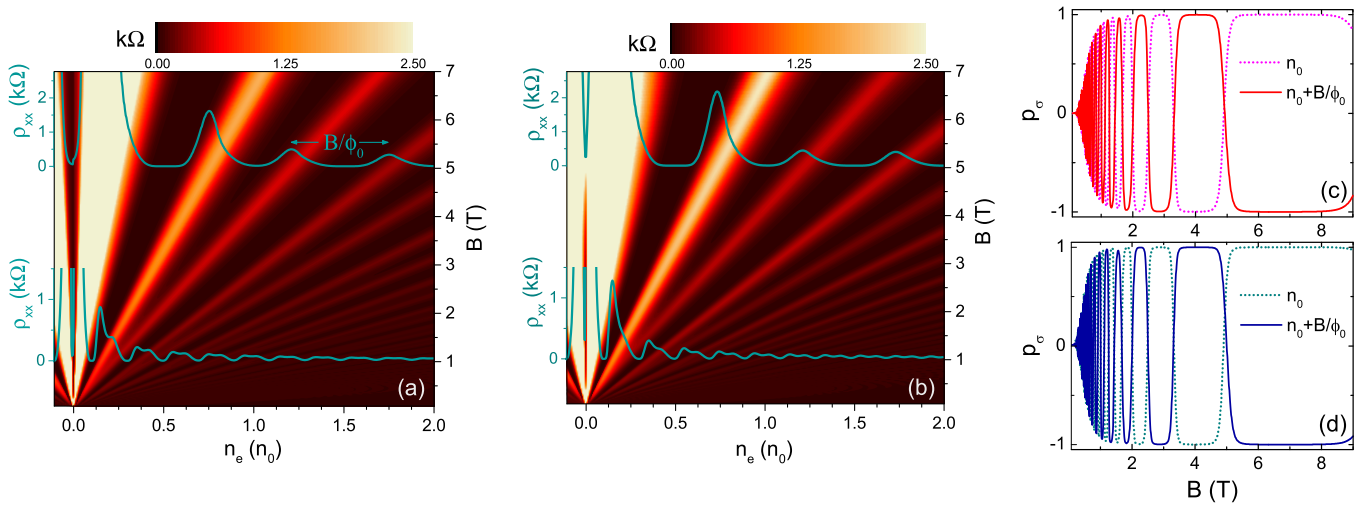

FIG. 2. (Color online) (a), (b) Resistivity fan chart versus the electron density and magnetic field for $d=55$ Å ($d<d_c$) and $d=70$ Å ($d>d_c$), respectively. The dimensionless broadening is $\Gamma=0.001$, $T=4.2$ K, and the scale of charge density is $n_0=2.42\times10^{11}$ cm^{-2}. The cyan curves show resistivity oscillations for magnetic fields $B=1$ T and $B=5$ T. The structure of these oscillations is very similar with the experimental results of Ref. [13] for $d=d_c$. (c), (d) Spin polarization of the longitudinal conductivity, p_σ, for the ordinary and inverted phases, respectively.

and inverted regimes. For nearly $B > 2$ T, each resistivity peak is tantamount to field-dependent electron density $n = (2\pi\ell_B^2)^{-1} = B/\phi_0$ [29], that is, the capacity of a single spin-resolved LL for filling with electrons. Therefore, as shown in Fig. 2(a), the Shubnikov–de Haas oscillation peaks are regularly spaced with period B/ϕ_0 for $B = 5$ T. By contrast, the low-field oscillations display a periodic dual-peak structure as seen for $B = 1$ T. The duality of the peaks can be traced to the fact that the spacing between spin-split LLs does not suffice to prevent the mixing of opposite spins. By enhancing the electron density and decreasing B, the peaks are gently quenched so that the oscillations are superficial. Note that the oscillatory structures shown for $B = 1$ T and $B = 5$ T, which are almost similar for $d > d_c$ and $d < d_c$, are qualitatively consistent with the experimental observations of Ref. [13] for $d = d_c$.

In support of the finding that claims that the magnetic field results in fully polarized spin excitations in magnetotransport, we show the spin polarization of the longitudinal conductivity by assessing the quantity $p_\sigma = (\sigma_{xx}^{\uparrow} - \sigma_{xx}^{\downarrow})/(\sigma_{xx}^{\uparrow} + \sigma_{xx}^{\downarrow})$. The results are summarized in Figs. 2(c) and 2(d) when the system is subject to the normal and inverted phases, respectively. As is evident, in both regimes, the function p_σ repeatedly changes its sign with magnetic field and exhibits perfect spin polarization for nearly $B > 1$ T. Furthermore, the dotted and solid curves, shown for constant and field-dependent ($n_e = n_0 + B/\phi_0$) densities, respectively, oscillate precisely out-of-phase. The reversal of the spin polarization p_σ means that the spin of the carriers near the Fermi level can be tuned by shifting the electron density by B/ϕ_0.

Figure 3 shows the Hall resistivity ρ_H as a function of the electron density n_e, in the inverted regime, for magnetic fields $B = 1$ T and $B = 5$ T. In essence, the transition regions between the standard plateaus are accompanied by resistivity peaks shown in Fig. 2(b). As a result, transitions occur in regular intervals of B/ϕ_0 revealing the reason why the plateaus are wide in the territory of Shubnikov–de Haas oscillations; see the red curve for $B = 5$ T. The value of the quantum Hall plateaus decreases continuously with steps located at $1/n$ (h/e^2) where n is an integer. These transitions are narrower in graphene by a factor of 1/4 because of spin and valley degeneracy of the LLs [30,31], and in addition the onset plateau occurs at 1/2 (h/e^2) since the $n = 0$ LL is only twice degenerate, and thus the resistance attains the quantized values $1/(4n + 2)$ (h/e^2). Notice that the $1/2n$ (h/e^2) transitions exist at low magnetic fields as long as there is spin resolution. Therefore, the pronounced transitions between the successive plateaus for $B = 5$ T correspond to different spin excitations which is an indication of strong spin splitting of the LLs. Conductivity measurements performed for LL spectroscopy of graphene [15,16] have shown splitting less than 1 meV in the field range $B \sim 0$ to $B = 18$ T. Here, the separation between opposite spins with the same LL index n is very large; e.g., Δ_s is about 1.5–3 meV for $B = 1$ T and 18–25 meV for $B = 10$ T. Therefore, it is expected that the spin-polarized excitations can be detected by magnetospectroscopy measurements for $B \gtrsim 1$ T.

The topologically distinct states of a HgTe QW have been shown to behave inconsistently in terms of the pseudospin configuration in the absence of a magnetic field [1,32]. Similarly, as mentioned earlier, by applying a magnetic field

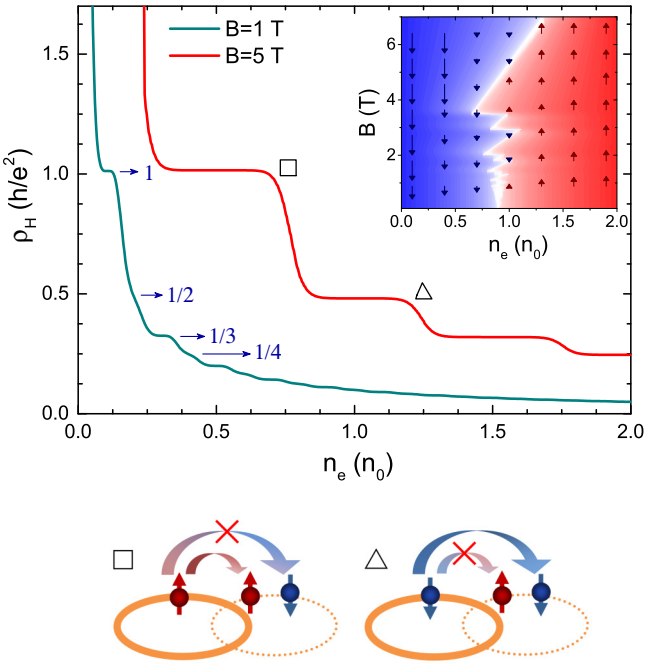

FIG. 3. (Color online) The Hall resistivity versus the electron density n_e for $d = 70$ Å. The contour plot shows the polarization extent of the conductivity in terms of pseudospin index and the blue and red colors correspond to ↓ and ↑ states, respectively. The arrows indicate the pseudospin texture of the electrons near the Fermi level. The lower sketches show schematically the initial and final spins for the scattering process of two transitions labeled by the □ and △ symbols.

the behavior of the pseudospin degree of freedom still separates between the topologically trivial and nontrivial regimes. In the topological phase, the pseudospin direction can be tuned via the density of charge carriers which is shown in the inset of Fig. 3. The white region corresponds to critical values of the magnetic field and electron density for which the pseudospin vanishes. Since this effect occurs only in the inverted regime, the pseudospin index can be viewed as an identification characteristic for the topologically separable phases.

IV. SUMMARY

We investigated the magnetotransport properties of HgTe QWs and showed that a fully spin-polarized quantum Hall liquid can be observed in the Shubnikov–de Haas regime when the system is in either the ordinary or inverted phases. This effect can experimentally be observed by magnetospectroscopy measurements for $B \gtrsim 1$ T. We also studied the pseudospin texture of the Fermi level electrons as well as the polarization extent of the conductivity in terms of the index τ, and showed that a tunable pseudospin-polarized quantum Hall liquid occurs only for the inverted regime. Both the spin and pseudospin polarizations are tunable by the electron density.

ACKNOWLEDGMENTS

This work was supported by the Flemish Science Foundation (FWO-Vl) and the Methusalem program of the Flemish government.

[1] B. A. Bernevig, T. L. Hughes, and S.-C. Zhang, Science **314**, 1757 (2006).
[2] M. König, S. Wiedmann, C. Brüne, A. Roth, H. Buhmann, L. Molenkamp, X.-L. Qi, and S.-C. Zhang, Science **318**, 766 (2007).
[3] M. König, H. Buhmann, L. W. Molenkamp, T. Hughes, C.-X. Liu, X.-L. Qi, and S.-C. Zhang, J. Phys. Soc. Jpn. **77**, 031007 (2008).
[4] C. L. Kane and E. J. Mele, Phys. Rev. Lett. **95**, 226801 (2005).
[5] D. Pesin and A. H. MacDonald, Nat. Mater. **11**, 409 (2012).
[6] J. E. Moore and L. Balents, Phys. Rev. B **75**, 121306 (2007).
[7] D. Hsieh, D. Qian, L. Wray, Y. Xia, Y. S. Hor, R. J. Cava, and M. Z. Hasan, Nature (London) **452**, 970 (2008).
[8] L. Fu and C. L. Kane, Phys. Rev. Lett. **100**, 096407 (2008).
[9] C. Brüne, C. X. Liu, E. G. Novik, E. M. Hankiewicz, H. Buhmann, Y. L. Chen, X. L. Qi, Z. X. Shen, S. C. Zhang, and L. W. Molenkamp, Phys. Rev. Lett. **106**, 126803 (2011).
[10] H. Jiang, S. Cheng, Q.-f. Sun, and X. C. Xie, Phys. Rev. Lett. **103**, 036803 (2009).
[11] A. Ström, H. Johannesson, and G. I. Japaridze, Phys. Rev. Lett. **104**, 256804 (2010).
[12] H.-H. Lee, J.-Y. Liu, C.-R. Chang, and S. Q. Shen, Phys. Rev. B **88**, 195149 (2013).
[13] B. Büttner, C. X. Liu, G. Tkachov, E. G. Novik, C. Brüne, H. Buhmann, E. M. Hankiewicz, P. Recher, B. Trauzettel, S. C. Zhang, and L. W. Molenkamp, Nat. Phys. **7**, 418 (2011).
[14] E. Tang and L. Fu, Nat. Phys. **10**, 964 (2014).
[15] Z. Jiang, E. A. Henriksen, L. C. Tung, Y.-J. Wang, M. E. Schwartz, M. Y. Han, P. Kim, and H. L. Stormer, Phys. Rev. Lett. **98**, 197403 (2007).
[16] M. L. Sadowski, G. Martinez, M. Potemski, C. Berger, and W. A. de Heer, Phys. Rev. Lett. **97**, 266405 (2006).
[17] E. O. Kane, J. Phys. Chem. Solids **1**, 249 (1957).
[18] X.-L. Qi and S.-C. Zhang, Rev. Mod. Phys. **83**, 1057 (2011).
[19] R. Kubo, J. Phys. Soc. Jpn. **12**, 570 (1957).
[20] G. D. Mahan, *Many-Particle Physics* (Plenum, New York, 1990).
[21] N. H. Shon and T. Ando, J. Phys. Soc. Jpn. **67**, 2421 (1998).
[22] G. D. Mahan, Phys. Rep. **145**, 251 (1987).
[23] G. Aarts and J. Berges, Phys. Rev. D **64**, 105010 (2001); A. A. Kovalev, Y. Tserkovnyak, K. Výborný, and J. Sinova, Phys. Rev. B **79**, 195129 (2009).
[24] Equation (5) can be derived after some algebra and using the identity "ET II 292(30)a" in Ref. [33].
[25] The derivation of Eq. (8) can be done in polar coordinates (q,θ). The integral over polar angle θ gives

$$\int e^{-\gamma(\mathbf{q}-\mathbf{q}')^2} e^{-q'^2} L_n(2q'^2) d\mathbf{q}'$$
$$= 2\pi e^{-\gamma q^2} \int_0^\infty e^{-(1+\gamma)q'^2} J_0(2i\gamma q q') L_n(2q'^2) q' dq',$$

where J_0 is the zero-order Bessel function of the first kind. Then, the identity "ET II 13(4)a" of Ref. [33] yields Eq. (8).
[26] V. P. Gusynin and S. G. Sharapov, Phys. Rev. Lett. **95**, 146801 (2005).
[27] B. Sacépé, J. B. Oostinga, J. Li, A. Ubaldini, N. J. G. Couto, E. Giannini, and A. F. Morpurgo, Nat. Commun. **2**, 575 (2011).
[28] A. K. Geim and I. V. Grigorieva, Nature (London) **499**, 419 (2013).
[29] M. O. Goerbig, Rev. Mod. Phys. **83**, 1193 (2011).
[30] Y. Zhang, Y.-W. Tan, H. L. Stormer, and P. Kim, Nature (London) **438**, 201 (2005).
[31] L. Zhang, Y. Zhang, J. Camacho, M. Khodas, and I. Zaliznyak, Nat. Phys. **7**, 953 (2011).
[32] S. Juergens, P. Michetti, and B. Trauzettel, Phys. Rev. Lett. **112**, 076804 (2014).
[33] I. S. Gradshteyn and I. M. Ryzhik, in *Table of Integrals, Series, and Products*, edited by A. Jeffrey and D. Zwillinger (Academic Press, San Diego, 2000).